# Highly Selective, Kinetically Driven Polymorphic Selection in Microfluidic Emulsion-Based Crystallization and Formulation

**ARTICLE** *in* CRYSTAL GROWTH & DESIGN · NOVEMBER 2014

Impact Factor: 4.89 · DOI: 10.1021/cg501222n



**8 AUTHORS**, INCLUDING:

Abu Zayed M Badruddoza
Massachusetts Institute of Technology
**23** PUBLICATIONS **469** CITATIONS
SEE PROFILE

Lu Zheng
National University of Singapore
**6** PUBLICATIONS **23** CITATIONS
SEE PROFILE

Eunice W.Q. Yeap
National University of Singapore
**1** PUBLICATION **2** CITATIONS
SEE PROFILE

Arpad I. Toldy
GlaxoSmithKline plc.
**6** PUBLICATIONS **30** CITATIONS
SEE PROFILE

CRYSTAL GROWTH & DESIGN

Article

pubs.acs.org/crystal

# Highly Selective, Kinetically Driven Polymorphic Selection in Microfluidic Emulsion-Based Crystallization and Formulation

Reno A. L. Leon,[†] Abu Zayed M. Badruddoza,[†] Lu Zheng,[†] Eunice W. Q. Yeap,[†] Arpad I. Toldy,[‡] Kay Yan Wong,[†] T. Alan Hatton,[‡,§] and Saif A. Khan*[,†,‡]

[†]Department of Chemical and Biomolecular Engineering, National University of Singapore, 4 Engineering Drive 4, Singapore 117576, Singapore

[‡]Chemical and Pharmaceutical Engineering Program, Singapore-MIT Alliance, National University of Singapore, 4 Engineering Drive 3, Singapore 117576, Singapore

[§]Department of Chemical Engineering, Massachusetts Institute of Technology, 77 Massachusetts Avenue, 66-309, Cambridge, Massachusetts 02139, United States

Supporting Information

**ABSTRACT:** We present a simple, potentially generalizable method to create highly monodisperse spherical microparticles (SMs) of ∼200 μm size containing active pharmaceutical ingredient (API) crystals and a macromolecular excipient, with unprecedented, highly specific, and selective control over the morphology and polymorphic outcome. The basic idea and novelty of our method is to control polymorphic selection within evaporating emulsion drops containing API−excipient mixtures via the kinetics of two simultaneously occurring processes: liquid−liquid phase separation and supersaturation generation, both governed by solvent evaporation. We demonstrate our method using two model hydrophobic APIs: 5-methyl-2-[(2-nitrophenyl)amino]-3-thiophenecarbonitrile (ROY) and carbamazepine (CBZ), formulated with ethyl cellulose (EC) as excipient. We dispense monodisperse oil-in-water (O/W) emulsions containing the API−excipient mixture on a flat substrate with a predispensed film of the continuous phase, which are subsequently subjected to evaporative crystallization. We are able to control the polymorphic selection by varying solvent evaporation rate, which can be simply tuned by the film thickness; thin (∼0.5 mm) and thick (∼2 mm) films lead to completely *specific* and *different* polymorphic outcomes for both model APIs: yellow (YT04) and orange (OP) for ROY, and form II and form III for CBZ respectively. Our method paves the way for simultaneous, bottom-up crystallization and formulation processes coupled with unprecedented polymorphic selection through process driven kinetics.

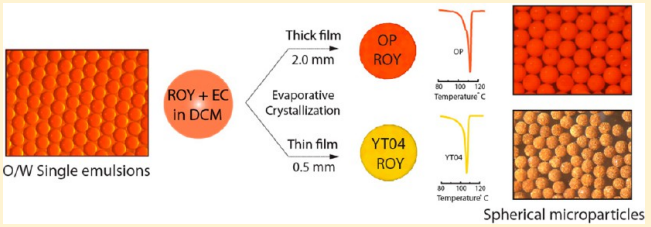


## INTRODUCTION

Polymorphism of pharmaceutical crystals, where the same drug molecule may exist in multiple possible crystalline structures, is a crucial consideration in pharmaceutical manufacturing since it directly influences the physicochemical properties and pharmacokinetic attributes of a drug, such as hardness, color, shelf life, dissolution rate, thermodynamic stability, and bioavailability.[1,2] This has prompted extensive experimental and theoretical research into the understanding and control of polymorphism in pharmaceutical crystals; several recent studies have explored a variety of means to direct polymorphism, including solvent-mediated polymorphic selection,[3] and selective polymorphic nucleation using tailor-made additives,[4] on self-assembled monolayers (SAMs),[5] in nanoscopic confinement,[6] in microgel particles,[7] on functionalized nanoparticles,[8] in emulsion droplets,[9] at oil−water interfaces,[10] and on excipient surfaces.[11] Despite significant progress in this area, directing and maintaining polymorphic purity, which is opposed by the phenomenon of concomitant polymorphism, is still a major challenge. Furthermore, maintaining crystal polymorphism during drug *formulation*, which involves multiple downstream secondary manufacturing operations, presents further challenges. Each downstream processing stage, from filtration to drying, size reduction, portioning, homogenizing, wet granulation, and compaction, presents a possibility for polymorphic transformation.[12−15] Since most active pharmaceutical ingredients (APIs) are complex organic molecules, the number of degrees of freedom in torsion angles and the molecule count per unit cell are frequently great, which can further lead to conformational polymorphism.[16] Thus, directing and also maintaining their polymorphic form, postsynthesis all the way through tableting, is a very challenging task.

We have recently demonstrated microfluidic emulsion-based crystallization to form monodisperse spherical agglomerates (SAs) of hydrophilic and hydrophobic model drug molecules (or their mixtures), with or without coformulated exci-

**Received:** August 18, 2014
**Revised:** November 19, 2014

   dx.doi.org/10.1021/cg501222n | *Cryst. Growth Des.* XXXX, XXX, XXX−XXX

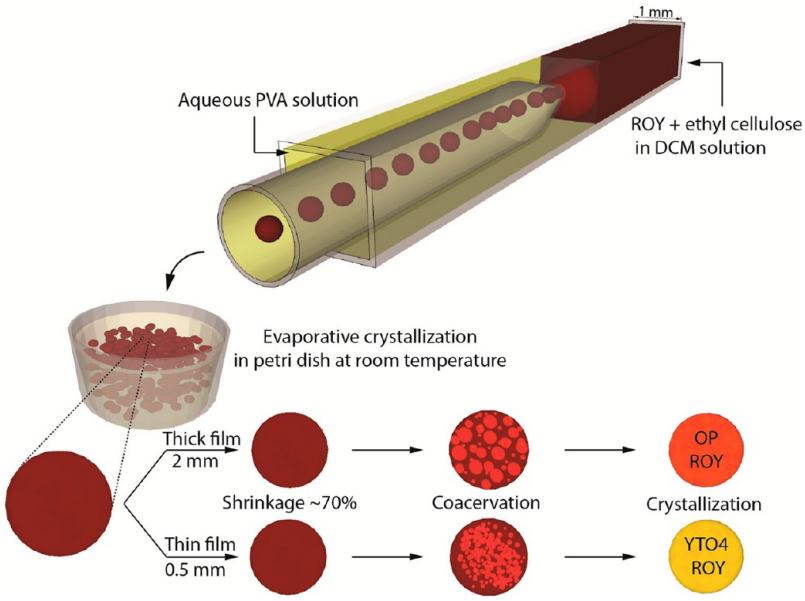


**Figure 1.** Schematic diagram of the experimental setup. Emulsion generation is performed in a concentric microfluidic glass capillary setup, where a square capillary (I.D. = 1 mm) houses a tapered round capillary (O.D. = 1 mm). The two ends of the square capillary function as inlets and the round capillary functions as a collection tube and outlet. The continuous phase (CP) of water (with dissolved surfactants) and a dispersed phase (DP) of ROY-EC in DCM solution are infused by syringe pumps into the square capillary. The emulsions are collected into a glass well (3.7 cm I.D.), where evaporative crystallization occurs.

pients.[17,18] The basic idea of our method is to generate monodisperse microfluidic emulsion drops containing API–excipient mixtures and to subsequently facilitate spherical crystallization within these drops via evaporative crystallization in thin films of the continuous phase. Our previous studies have demonstrated excellent control over the structure and morphology of the spherical agglomerates, albeit with limited polymorphic selectivity. Here we focus on polymorphic selection and present a simple, potentially generalizable method to create highly monodisperse, *bottom-up* formulated spherical microparticles (~200 $\mu$m) containing API crystals and a macromolecular excipient, with unprecedented, nearly complete, and tunable control over the morphology and polymorphic outcome. The novelty of our method is in controlling polymorphic selection via the *kinetics* of two simultaneous processes occurring within evaporating emulsion drops containing API–excipient mixtures: (i) liquid–liquid phase separation, which *compartmentalizes* the API while also provides sites for heterogeneous polymorphic nucleation and (ii) increasing supersaturation of both the API and excipient-rich phases, eventually leading to solidification of the excipient, which further facilitates nucleation and crystallization of the API.

We demonstrate our method using two model hydrophobic APIs: 5-methyl-2-[(2-nitrophenyl)amino]-3-thiophenecarbonitrile (also known as "ROY", due to the characteristic color of its polymorphs) and carbamazepine (CBZ), formulated with ethyl cellulose (EC) as excipient. ROY and CBZ both exhibit conformational polymorphism, with 10 and 4 known polymorphs, respectively.[10,19] In our method, an API–excipient solution in the solvent dichloromethane (DCM) is used to form oil-in-water (O/W) emulsions with an aqueous solution of poly(vinyl alcohol) (PVA) serving as the continuous phase, in a microcapillary emulsion generator. This is followed by thin-film evaporation, similar to the methodology of our recent work cited above (Figure 1).[17,18] Remarkably, we are able to control the polymorphic selection by varying the solvent evaporation rate, which is simply tuned by the film *thickness*; fast (film thickness ~0.5 mm, the thinnest we can achieve without breaking the emulsions) and slow (film thickness ~2 mm) lead to completely *specific* and *different* polymorphic outcomes for both model APIs—yellow (YT04) and orange (OP) for ROY, and form II and form III for CBZ respectively. We further explain our observations in terms of interplay between simultaneous dynamic processes within the evaporating emulsion drops. Our method thus paves the way for simultaneous, bottom-up crystallization and formulation processes coupled with unprecedented polymorphic selection through process driven kinetics. We envision it to form the basis of simple, robust, and sustainable process platforms for continuous pharmaceutical drug particle manufacturing.

## EXPERIMENTAL SECTION

**Materials.** Poly(vinyl) alcohol (PVA) (M.W. 67,000), dichloromethane (DCM) (99.5%), EC (viscosity 10 cP) and CBZ were purchased from Sigma-Aldrich (Singapore) and used as received. 5-Methyl-2-[(2-nitrophenyl)amino]-3-thiophenecarbonitrile (ROY) was purchased from Nanjing Chemlin Chemical Industry Co. Ltd., China. Ultrapure water (18.3 MΩ) obtained using a Millipore Milli-Q purification system was used to prepare aqueous PVA solution. Harvard PHD 22/2000 series syringe pumps were used to dispense fluids into the emulsion generator. Square and cylindrical glass capillaries of I.D. 1 mm and 0.7 mm respectively were purchased from Arte glass associates Co. Ltd., Japan.

**Methods.** O/W emulsions were generated using a glass capillary microfluidic setup (Figure 1). The axisymmetric coaxial glass capillary flow-focusing device was assembled using square and round capillaries. The surface of the round capillary was hydrophilized with treatment by oxygen plasma (100 W) for 120 s. The aqueous continuous phase (W) was prepared by mixing 1.5 wt % PVA in water. The dispersed phase (O) was one of the following four: (i) ROY in DCM (400 mg/mL), (ii) ROY-EC in DCM (320 and 80 mg/mL, respectively), (iii) CBZ-EC in DCM (68 and 17 mg/mL, respectively), (iv) CBZ in DCM (140 mg/mL, respectively). W and O phases were infused from the


dx.doi.org/10.1021/cg501222n | *Cryst. Growth Des.* XXXX, XXX, XXX–XXX

two ends of the square capillary through the outer coaxial region using syringe pumps (Harvard PHD 22/2000 series) at flow rates of 150 and 50 $\mu$L/min, respectively. The fluids were hydrodynamically flow focused through the nozzle of the round capillary resulting in the formation of the emulsion drops (see Supporting Information Figure S1). 3.7 cm I.D. glass wells were used for sample collection and as crystallization platforms. Approximately 100 $\mu$L of O/W emulsions was dispensed directly into the glass well containing either a "thin" (0.5 mm) or "thick" (2 mm) film of the continuous phase. Change in film thickness of the predispensed film was 0.09 mm upon addition of the emulsion droplets into the collection well. Evaporative crystallization was performed at room temperature (24 °C) and at ambient humidity (55%). Optical microscopy images were captured using a Qimaging MicroPublisher 5.0 RTV camera mounted on an Olympus SZX7 microscope. A Leica CLS 150 XE light source was used. A thin film of continuous phase persisted at the end of all experiments and was measured to be 0.49 mm after 45 min and 1.95 mm after 2 h, for the thin and thick film cases, respectively.

**Characterization.** The size distribution, morphology, and polymorphism of the SMs obtained were characterized by using microscopic image analysis, field emission scanning electron microscopy (FESEM), powder X-ray diffraction (PXRD), and differential scanning calorimetry (DSC). For the size distribution studies we used an inverted microscope (Nikon Eclipse Ti) operated in bright field mode. The inbuilt software (NIS Elements 3.22.0) was used to measure the diameters of the agglomerates (circle by a three points method) and to estimate the average diameters and standard deviations based on measurements of at least 100 SMs. A field emission scanning electron microscope (JEOL JSM-6700F) at 5 kV accelerating voltage was used to acquire further structural information on the SMs. All samples were prepared on conventional SEM stubs with carbon tape and were coated with ~10 nm of platinum by sputter coating. An XRD diffractometer (LabX XRD-6000, Shimadzu) with characteristic Cu radiation was used for polymorphic characterization. The X-ray diffractometer was operated at 40 kV, 30 mA, and at a scanning rate of 2°/min over the range of $2\theta$ = 10−40°, using the Cu radiation wavelength of 1.54 Å. The DSC thermograms were obtained using a Mettler Toledo DSC 882 apparatus. Around 5 mg of sample was crimped in a sealed aluminum pan and heated at 5 °C/min in the range of room temperature to 225 °C using an empty sealed pan as a reference. Dry nitrogen was used as purge gas and the $N_2$ flow rate was 50 mL/min. The DSC instrument has a signal-to-noise ratio of ~12 (see Supporting Information for further details).

## RESULTS AND DISCUSSION

Emulsions of ROY-EC in DCM (100 $\mu$L) were dispensed into a glass well containing a predispensed film of water−PVA solution (0.5 and 2 mm nominal film thickness) for subsequent evaporative crystallization. The entire crystallization process took ~40 min and ~4 h for thin and thick film cases, respectively, at ambient temperature (24 °C). Monodisperse SMs of ROY-EC of diameter 180 $\mu$m (with a standard deviation of 5%) were produced under both conditions. Polymorphic selection of nearly 100% was achieved for both conditions, as indicated by particle color and the DSC characterization (Figure 2); yellow and orange microparticles were obtained for the thin and thick film cases, respectively. DSC characterization reveals the yellow polymorph to be YT04 and the orange polymorph to be orange plate (OP); here we note that YT04 is thermodynamically less stable than OP among the reported polymorphs of ROY at room temperature.[20] Figure 3 compares electron microscopy (FESEM) images of the structure of YT04 and OP SMs, highlighting the spherical shape of particles obtained in both cases. Further, FESEM images also reveal interesting structural differences between the two cases. YT04 particles have a compact structure that consists of polycrystalline, presumably spherulitic domains

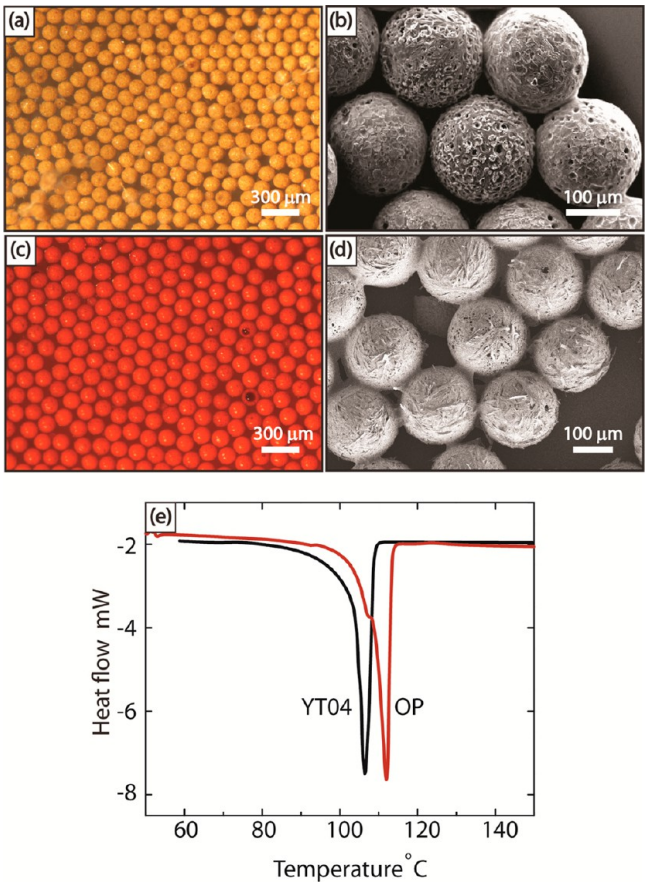


**Figure 2.** (a, c) Optical and (b, d) FESEM images of microparticles containing ROY and EC for the "thin" (0.5 mm) and "thick" (2 mm) film scenarios, respectively. The drug-excipient loading ratio is 4:1 (320 mg of ROY: 80 mg of EC) for both cases. (e) Differential scanning calorimetry (DSC) profiles for the particles with endotherms at 106.9 and 112.7 °C corresponding to the yellow needle (YT04) and orange plate (OP) polymorphs of ROY respectively.[10,20]

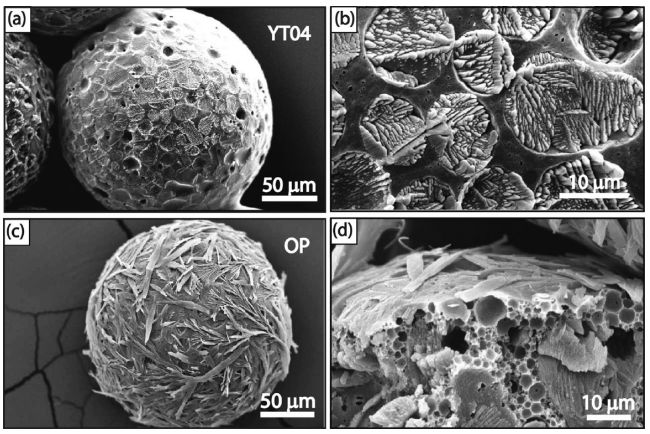


**Figure 3.** Representative FESEM images of ROY-EC microparticles from thin and thick film experiments: (a, b) YT04 particles displaying a compact, cellular structure with an EC scaffold harboring polycrystalline ROY domains, and (c, d) orange plate (OP) ROY particles displaying plate like crystals on the surface and within "the domains" surrounded by a porous EC scaffold.

tightly embedded within an EC matrix—a YT04 morphology previously observed by Sun et al.,[21,22] whereas OP particles exhibit a void-filled porous structure with large single crystals


dx.doi.org/10.1021/cg501222n | Cryst. Growth Des. XXXX, XXX, XXX−XXX

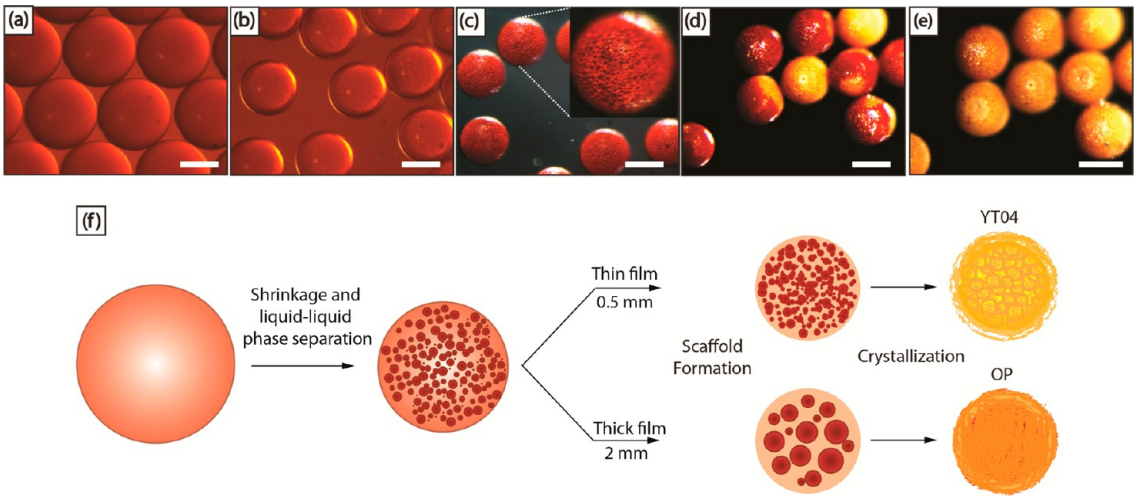


**Figure 4.** (a–e) Time lapse stereomicroscopic images of emulsion drops subjected to evaporative crystallization under the thin film (0.5 mm) condition. Images were taken at intervals of 10 min each. (f) A phenomenological schematic capturing the various stages in the microparticle formation process, including solvent evaporation/shrinkage, liquid–liquid phase separation, EC scaffold formation and crystallization. All scale bars represent 100 $\mu$m.

loosely encapsulated within the pores and ribbon-like crystal flakes covering the particle surfaces.

To better understand the particle formation process, we conducted online optical microscopic monitoring of the entire crystallization process. As shown in Figure 4a–e, which are time-lapse optical microscopic images of evaporating emulsion drops, we note the occurrence of a liquid–liquid phase separation of the three component (ROY-EC-DCM) system as the solvent (DCM) evaporates. Small droplets ("domains") were observed to form within the dispensed droplets and grow in size over time. The average domain size measured immediately after the first crystallization event in the droplet ensemble for the thin film case (3 $\mu$m) was smaller than that observed in the thick film experiments (12 $\mu$m), indicating coarsening of the domains in the latter case. As suggested by the FESEM images in Figure 3, ROY crystals formed the major component in these domains, whereas EC formed an interconnected scaffold surrounding the domains.

We interpret and explain our observations in terms of an interplay between simultaneous dynamic processes occurring within the evaporating emulsion drops containing API–excipient mixtures: (i) liquid–liquid phase separation of the three component system, API–excipient–solvent, due to solvent evaporation, which *compartmentalizes* the API-rich solution into small domains surrounded by the excipient, which then provides surfaces for heterogeneous nucleation of the API (see Discussion below) and (ii) increasing supersaturation of both the API and excipient rich phases, eventually leading to solidification of the excipient, which further facilitates crystallization of API. We roughly estimate the saturation concentration of ROY in DCM to be around 570 mg/mL. Assuming droplet shrinkage of ~70% and no ROY leaving the droplets, we calculate the supersaturation within the shrunk droplets to be ~1.7 for both thin and thick film conditions. For the thin film case, due to fast evaporation and supersaturation generation (data from droplet shrinkage measurements are provided in the Supporting Information, Figure S2), the domains form rapidly (within ~3 min), resulting in a population of highly supersaturated internal droplets, where conditions are conducive to spherulitic growth.[23,24] On the other hand, in the case of thick films, slow evaporation results in a milder temporal supersaturation profile and the possible coarsening of the domains. Polymorphic selectivity in confined spaces, governed by the temporal supersaturation profile, has been previously reported in the context of aqueous glycine solutions by Kim et al.[5] In their study, aqueous glycine solutions confined to small droplets were evaporated at different rates, and a higher rate of evaporation (i.e., rate of supersaturation generation) resulted in the formation of the less stable $\beta$ polymorph, whereas the more stable $\alpha$ polymorph was obtained at slower evaporation rates.[5] Another study by Singh et al., which focused on evaporative crystallization of ROY from sessile drops on a patterned surface, demonstrated polymorphic selection by kinetic means, where a decrease in droplet size led to a faster supersaturation generation, resulting in higher percentages of less stable polymorphs.[25] Our observation of the less stable YT04 polymorph[26] appearing at higher evaporation rates and the comparatively more stable OP polymorph crystallizing under a slow rate of supersaturation generation in confined spaces is therefore consistent with previous reports.

To further investigate and validate the crucial role of the excipient, we compare and contrast the above results with the case of ROY crystallization in the absence of EC. 100 $\mu$L of emulsions generated from ROY-DCM solution in aqueous PVA solution were dispensed into a glass well containing a predispensed film of water–PVA solution (0.5 and 2 mm film thickness) for subsequent evaporative crystallization. As compared to the case with excipient, relatively fewer monodisperse and irregular shaped particles of ROY were formed under both the thin and thick film conditions (Figure 5). The time taken for particle formation was ~1.5 h and ~7 h for the thin and thick film cases respectively, which is 2–3 times longer than the above cases where EC was used along with ROY. Optical microscopy images of the ROY microparticles indicate concomitant polymorphism and thus poor control over polymorphic selection (Figure 5); DSC characterization further confirms the concomitant occurrence of both YT04 and OP polymorphs.

Liquid–liquid phase separation was also observed in this case (Figure 6); small ROY precipitates were seen appearing and growing inside the emulsion droplets within ~1 min after dispensing. In the case of an API–solvent system, this phase


dx.doi.org/10.1021/cg501222n | *Cryst. Growth Des.* XXXX, XXX, XXX–XXX

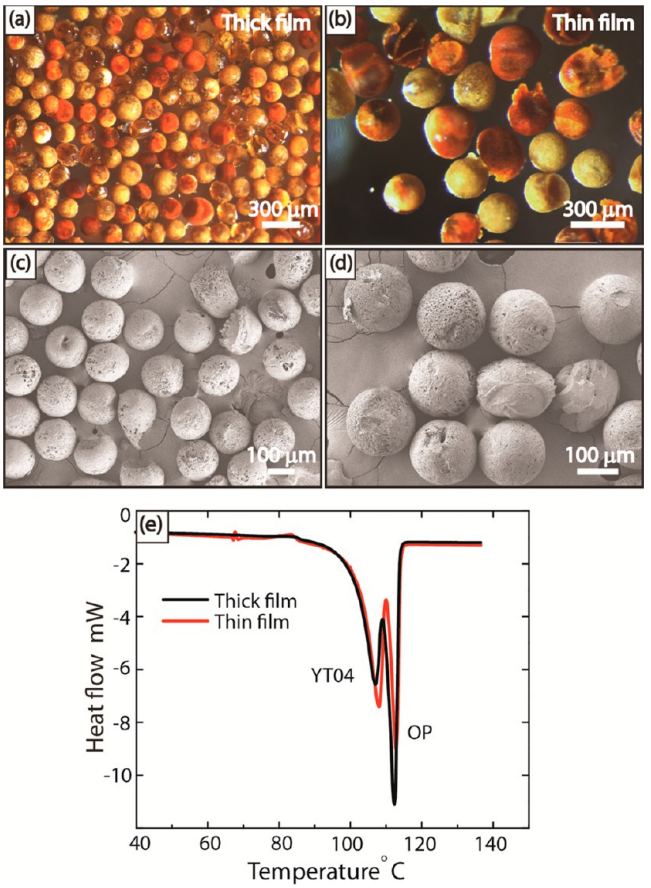


**Figure 5.** Optical (a, b) and FESEM (c, d) images of pure ROY (400 mg/mL) microparticles: a mixture of yellow, orange, and brown particles indicate poor polymorphic selectivity; (e) DSC profiles indicating concomitant polymorphism of YT04 and OP polymorphs of ROY for both thin (0.5 mm) and thick film (2 mm) conditions.

separation is known as "oiling out" and is commonly observed during the crystallization of small organic molecules.[27,28] Here, the solute−solvent system transitions from a single liquid phase into a metastable liquid−liquid state (having a solute-rich and solute-lean phase), bypassing the solid−liquid zone in the phase diagram altogether.[27] Recent pharmaceutical development has seen an increase in the number of lipophilic and nonpolar API molecules,[9] such as ROY, which do not easily self-assemble and are prone to liquid−liquid phase separation.[25,29] Further, the metastable liquid−liquid state is known to hinder primary and secondary nucleation, leading to long crystallization process times of up to 35 h;[30] often, special measures are needed to move the system away from this part of the phase diagram to promote nucleation and growth of crystals.[27,29−31] This is in keeping with our observations of longer crystallization times for this case, as compared to the results with excipient. In the latter case, the formation of an excipient scaffold upon solvent evaporation provided heterogeneous sites for nucleation of ROY crystals in both the thin and thick film cases, the polymorphism ultimately being dictated by the different temporal rates of supersaturation generation, as discussed above.

Finally, to validate the core idea, we demonstrate controlled polymorphic selection of another model molecule—carbamazepine (CBZ)—an anticonvulsant that has multiple polymorphic forms via conformational polymorphism. An analogous protocol was followed in this case; droplets of CBZ in DCM were generated in an aqueous PVA continuous phase, and subjected to evaporative crystallization in both thin (0.5 mm) and thick films (2 mm), as for the case of ROY. Droplet shrinkage was ∼70% for both cases. On the basis of the saturation concentration of CBZ in DCM (158 mg/mL),[32] and the solute concentration within the shrunk droplets (182 mg/mL), the supersaturation was estimated to be ∼1.2. The particles generated were highly monodisperse and had a smooth surface morphology. Electron microscopy of broken sections of the particles show needle-shaped CBZ crystals trapped within the porous framework of ethyl cellulose (Figure 7) in both cases. Powder X-ray diffraction (XRD) characterization reveals that particles from the thin and thick film experiments correspond to least stable form II and most stable form III polymorphs of CBZ (form II < IV < I < III) respectively.[19] As indicated in Figure 7g [(i) and (ii)], major peaks identified at 13.26°, 18.56°, and 24.54° are attributed to form II CBZ and peaks at 15.36°, 19.56°, 25.00°, and 27.47° to form III CBZ, respectively.[19] Dominant and unrepeated occurrence of characteristic peaks corresponding to the two forms of CBZ provides strong evidence of polymorphic selection using our method. Finally, DSC analysis was performed to validate polymorphic selection of CBZ determined by XRD, showing form II under thin film and form III under thick film. DSC thermograms were recorded at 5 °C/min from 25 to 225 °C, corresponding to the melting range of CBZ forms (Figure 7h).[19] An endotherm at 188 °C for the sample from the thin film experiment confirmed the presence of form II CBZ polymorph, which has a reported melting point in the range of 188−192 °C. The endotherm at 192 °C for CBZ samples from the thick film experiment confirmed the presence of form III CBZ polymorph, which has a reported melting point in the range of 189−193 °C.[19] DSC thermograms thus reinforced our XRD results, providing strong validation for polymorphic selection of CBZ.

Similar to ROY, pure CBZ was crystallized in the absence of EC to verify the role of excipient (see Supporting Information). Pure CBZ particles obtained were irregular in shape (mostly needles) and polydisperse under both thin and thick film

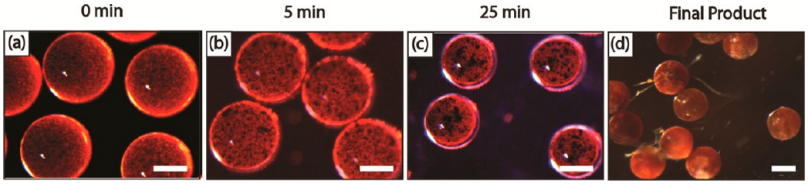


**Figure 6.** (a−d) Time-lapse stereomicroscopic images of ROY-DCM emulsion drops subjected to evaporative crystallization under the thin film (0.5 mm) condition. Droplet shrinkage followed by oiling out of ROY from DCM and subsequent crystallization was observed. All scale bars represent 100 $\mu$m.


dx.doi.org/10.1021/cg501222n | *Cryst. Growth Des.* XXXX, XXX, XXX−XXX

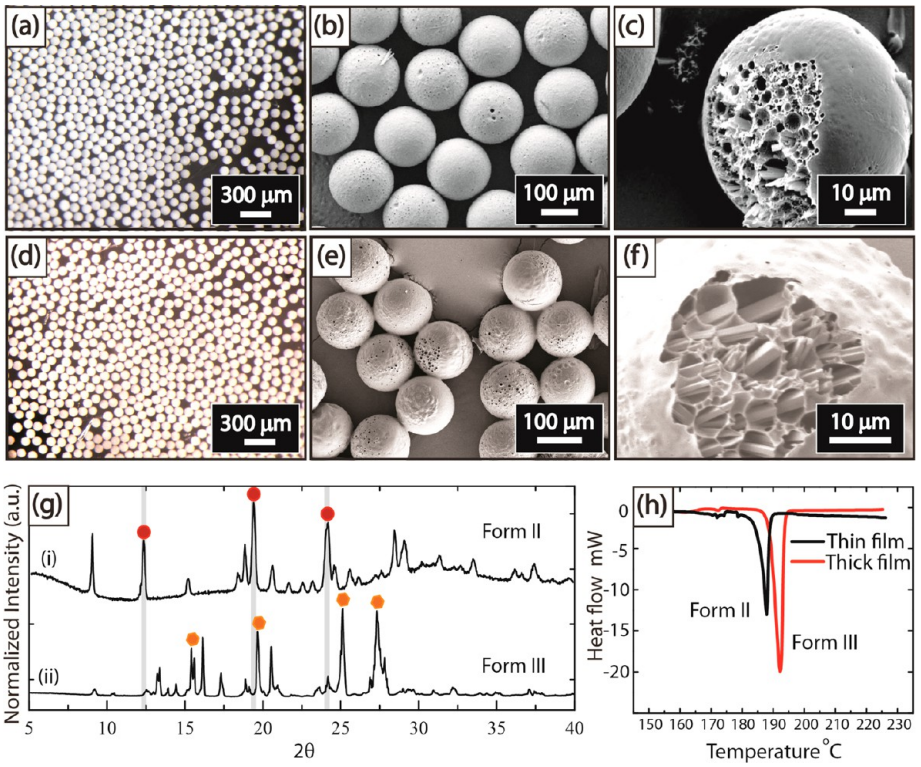


**Figure 7.** Optical and FESEM images of CBZ-EC microparticles from thin and thick film experiments: (a, b, d, e) monodisperse population of particles with a smooth surface morphology and (c, f) broken cross section of particle displaying needle shaped crystals embedded in the porous excipient matrix. (g) XRD patterns corresponding to form II and form III polymorphs of CBZ obtained for the thin and thick film cases, respectively. (h) DSC profiles for thin film and thick film cases: characteristic endotherms for form II and form III polymorphs of CBZ are found at 188 and 192 °C respectively.[19]

conditions. PXRD characterization revealed concomitant occurrence of form I, form II and form III polymorphs of CBZ confirming poor control over polymorphic selection in the absence of EC for both thin and thick film conditions.

## CONCLUSIONS

Our ongoing work beyond this initial proof-of-concept demonstration involves detailed studies of the dynamics of crystallization in this chemically complex emulsion system. The compositional characterization of domains formed within emulsion drops and the mechanism of particle formation, including the influence of the excipient on the morphological and polymorphic outcome (API−excipient interaction and surface-induced nucleation kinetics),[11] are of particular interest. Moreover, a broad and detailed study on how film thickness and droplet size affect solvent evaporation rate and supersaturation generation in emulsion drops, thus dynamics of the system, and eventually crystallization outcomes, is worth pursuing. In summary, we present a simple, potentially generalizable method to create monodisperse spherical microparticles (~200 $\mu$m) containing pharmaceutical crystals and a macromolecular excipient, with unprecedented, highly specific, and selective control over the polymorphic outcome. Online monitoring enabled by the platform makes in-depth understanding of particle formation process possible, where we further explain our observations in terms of an interplay between simultaneous dynamic processes within the evaporating emulsion drops. The platform enables novel means of formulation and crystallization, with the ability to control crystal polymorphism without the aid of sophisticated external alternatives. We envision it to form the basis of simple, robust, and sustainable process platforms for continuous pharmaceutical particle manufacturing.

## ASSOCIATED CONTENT

### Supporting Information

Experimental details. Figure S1: (a) Single emulsion generation at the tip of the inner round glass capillary of a microfluidic device operating at a flow focusing configuration. Stereomicroscopic images of dispensed (b) ROY-EC-DCM emulsion droplets and (c) CBZ-EC-DCM emulsions droplets. Figure S2: Droplet size measurements over time under thin film (0.5 mm) and thick film (2.0 mm). Figure S3: DSC profile with endotherms at 107.6 °C and 112 °C corresponding to a polymorphic mixture of YT04 (99 wt%) and OP (1 wt%) respectively. Figure S4: (a, b) Stereomicroscopic images of CBZ (140 mg/mL) microparticles, crystallized in the absence of EC, showing irregular needle shaped morphology for both thin and thick film conditions; (c) PXRD profiles indicating concomitant polymorphism of form I, form II, and form III CBZ for both thin (0.5 mm) and thick film (2 mm) conditions. Figure S5: DSC profile for pure CBZ sample showing characteristic endotherm for form I polymorph at 192 °C. This material is available free of charge via the Internet at http://pubs.acs.org.

## AUTHOR INFORMATION

### Corresponding Author

*E-mail: saifkhan@nus.edu.sg.



dx.doi.org/10.1021/cg501222n | *Cryst. Growth Des.* XXXX, XXX, XXX−XXX

### Notes

The authors declare no competing financial interest.

## ■ ACKNOWLEDGMENTS

The authors gratefully acknowledge research funding from the GSK-EDB Fund for Sustainable Manufacturing and the Chemical and Pharmaceutical Engineering Programme of the Singapore−MIT Alliance.

## ■ REFERENCES

(1) Mangin, D.; Puel, F.; Veesler, S. Polymorphism in Processes of Crystallization in Solution: A Practical Review. *Org. Process Res. Dev.* **2009**, *13* (6), 1241−1253.
(2) Blagden, N.; De Matas, M.; Gavan, P. T.; York, P. Crystal engineering of active pharmaceutical ingredients to improve solubility and dissolution rates. *Adv. Drug Delivery Rev.* **2007**, *59* (7), 617−630.
(3) Weissbuch, I.; Torbeev, V. Y.; Leiserowitz, L.; Lahav, M. Solvent Effect on Crystal Polymorphism: Why Addition of Methanol or Ethanol to Aqueous Solutions Induces the Precipitation of the Least Stable $\beta$ Form of Glycine. *Angew. Chem., Int. Ed.* **2005**, *44* (21), 3226−3229.
(4) Weissbuch, I.; Addadi, L.; Leiserowitz, L. Molecular Recognition at Crystal Interfaces. *Science* **1991**, *253* (5020), 637−645.
(5) Kim, K.; Centrone, A.; Hatton, T. A.; Myerson, A. S. Polymorphism control of nanosized glycine crystals on engineered surfaces. *CrystEngComm* **2011**, *13* (4), 1127−1131.
(6) Ha, J.-M.; Wolf, J. H.; Hillmyer, M. A.; Ward, M. D. Polymorph Selectivity under Nanoscopic Confinement. *J. Am. Chem. Soc.* **2004**, *126* (11), 3382−3383.
(7) Diao, Y.; Whaley, K. E.; Helgeson, M. E.; Woldeyes, M. A.; Doyle, P. S.; Myerson, A. S.; Hatton, T. A.; Trout, B. L. Gel-Induced Selective Crystallization of Polymorphs. *J. Am. Chem. Soc.* **2011**, *134* (1), 673−684.
(8) Md. Badruddoza, A. Z.; Toldy, A. I.; Hatton, T. A.; Khan, S. A. Functionalized Silica Nanoparticles as Additives for Polymorphic Control in Emulsion-Based Crystallization of Glycine. *Cryst. Growth Des.* **2013**, *13* (6), 2455−2461.
(9) Stahl, P. H.; Wermuth, C. G. *Pharmaceutical Salts: Properties, Selection, and Use*; John Wiley & Sons: New York, 2002.
(10) Yu, L. Polymorphism in molecular solids: an extraordinary system of red, orange, and yellow crystals. *Acc. Chem. Res.* **2010**, *43* (9), 1257−1266.
(11) Quon, J. L.; Chadwick, K.; Wood, G. P. F.; Sheu, I.; Brettmann, B. K.; Myerson, A. S.; Trout, B. L. Templated Nucleation of Acetaminophen on Spherical Excipient Agglomerates. *Langmuir* **2013**, *29* (10), 3292−3300.
(12) Andrews, G. P. Advances in solid dosage form manufacturing technology. *Philos. Trans. R. Soc., A* **2007**, *365* (1861), 2935−2949.
(13) Morris, K. R.; Griesser, U. J.; Eckhardt, C. J.; Stowell, J. G. Theoretical approaches to physical transformations of active pharmaceutical ingredients during manufacturing processes. *Adv. Drug Delivery Rev.* **2001**, *48* (1), 91−114.
(14) Kaneniwa, N.; Otsuka, M. Effect of grinding on the transformations of polymorphs of chloramphenicol palmitate. *Chem. Pharm. Bull.* **1985**, *33* (4), 1660−1668.
(15) Bauer-Brandl, A. Polymorphic transitions of cimetidine during manufacture of solid dosage forms. *Int. J. Pharm.* **1996**, *140* (2), 195−206.
(16) Morissette, S. L.; Almarsson, Ö.; Peterson, M. L.; Remenar, J. F.; Read, M. J.; Lemmo, A. V.; Ellis, S.; Cima, M. J.; Gardner, C. R. High-throughput crystallization: polymorphs, salts, co-crystals and solvates of pharmaceutical solids. *Adv. Drug Delivery Rev.* **2004**, *56* (3), 275−300.
(17) Toldy, A. I.; Badruddoza, A. Z. M.; Zheng, L.; Hatton, T. A.; Gunawan, R.; Rajagopalan, R.; Khan, S. A. Spherical Crystallization of Glycine from Monodisperse Microfluidic Emulsions. *Cryst. Growth Des.* **2012**, *12* (8), 3977−3982.
(18) Leon, R. A. L.; Wan, W. Y.; Badruddoza, A. Z. M.; Hatton, T. A.; Khan, S. A. Simultaneous Spherical Crystallization and Co-Formulation of Drug(s) and Excipient from Microfluidic Double Emulsions. *Cryst. Growth Des.* **2013**, *14* (1), 140−146.
(19) Grzesiak, A. L.; Lang, M.; Kim, K.; Matzger, A. J. Comparison of the four anhydrous polymorphs of carbamazepine and the crystal structure of form I. *J. Pharm. Sci.* **2003**, *92* (11), 2260−2271.
(20) Chen, S.; Guzei, I. A.; Yu, L. New Polymorphs of ROY and New Record for Coexisting Polymorphs of Solved Structures. *J. Am. Chem. Soc.* **2005**, *127* (27), 9881−9885.
(21) Sun, Y.; Xi, H.; Chen, S.; Ediger, M. D.; Yu, L. Crystallization near Glass Transition: Transition from Diffusion-Controlled to Diffusionless Crystal Growth Studied with Seven Polymorphs. *J. Phys. Chem. B* **2008**, *112* (18), 5594−5601.
(22) Sun, Y.; Zhu, L.; Wu, T.; Cai, T.; Gunn, E.; Yu, L. Stability of Amorphous Pharmaceutical Solids: Crystal Growth Mechanisms and Effect of Polymer Additives. *AAPS J.* **2012**, *14* (3), 380−388.
(23) Goldenfeld, N. Theory of spherulitic crystallization. *J. Cryst. Growth* **1987**, *84* (4), 601−608.
(24) Gránásy, L.; Pusztai, T.; Tegze, G.; Warren, J. A.; Douglas, J. F. Growth and form of spherulites. *Phys. Rev. E* **2005**, *72* (1), 011605.
(25) Singh, A.; Lee, I. S.; Myerson, A. S. Concomitant Crystallization of ROY on Patterned Substrates: Using a High Throughput Method to Improve the Chances of Crystallization of Different Polymorphs. *Cryst. Growth Des.* **2008**, *9* (2), 1182−1185.
(26) Chen, S.; Xi, H.; Yu, L. Cross-Nucleation between ROY Polymorphs. *J. Am. Chem. Soc.* **2005**, *127* (49), 17439−17444.
(27) Bonnett, P.; Carpenter, K.; Dawson, S.; Davey, R. Solution crystallisation via a submerged liquid−liquid phase boundary: oiling out. *Chem. Commun.* **2003**, *6*, 698−699.
(28) Lafferrère, L.; Hoff, C.; Veesler, S. In situ monitoring of the impact of liquid-liquid phase separation on drug crystallization by seeding. *Cryst. Growth Des.* **2004**, *4* (6), 1175−1180.
(29) Derdour, L. A method to crystallize substances that oil out. *Chem. Eng. Res. Des.* **2010**, *88* (9), 1174−1181.
(30) Veesler, S.; Revalor, E.; Bottini, O.; Hoff, C. Crystallization in the presence of a liquid-liquid phase separation. *Org. Process Res. Dev.* **2006**, *10* (4), 841−845.
(31) Kim, S.; Wei, C.; Kiang, S. Crystallization process development of an active pharmaceutical ingredient and particle engineering via the use of ultrasonics and temperature cycling. *Org. Process Res. Dev.* **2003**, *7* (6), 997−1001.
(32) Jouyban, A. *Handbook of Solubility Data for Pharmaceuticals*; CRC Press: Boca Raton, FL, 2010.